11-11-2009

Strong Southward Transport Events Due to Typhoons in the Taiwan Strait

W. Z. Zhang

H. H. Hong

S. P. Shang

X. H.C. Yan

Fei Chai
University of Maine - Main, fchai@maine.edu

Strong southward transport events due to typhoons in the Taiwan Strait

Wen-Zhou Zhang,[1,2,3] Hua-Sheng Hong,[1] Shao-Ping Shang,[2] Xiao-Hai Yan,[1,3] and Fei Chai[4]

Received 10 March 2009; revised 27 July 2009; accepted 3 August 2009; published 11 November 2009.

[1] Transport through the Taiwan Strait under the influence of five typhoons was investigated using both buoy observations and numerical model simulations during the period of 27 August to 5 October 2005. The results show that the effects of typhoons on the Taiwan Strait and its adjacent sea area caused strong southward transport events in the Taiwan Strait, which changed the direction of the Taiwan Strait northward transport temporarily. Typhoon-generated local wind stress and/or along-strait water level gradient were the direct driving factors in these southward transport events. The numerical results show that the Coriolis force made a negative contribution to these events and the contribution of the along-strait momentum gradient was insignificant.

Citation: Zhang, W.-Z., H.-S. Hong, S.-P. Shang, X.-H. Yan, and F. Chai (2009), Strong southward transport events due to typhoons in the Taiwan Strait, *J. Geophys. Res.*, *114*, C11013, doi:10.1029/2009JC005372.

1. Introduction

[2] The Taiwan Strait, which is located on the wide continental shelf of the China Seas, is a long, shallow channel connecting the East China Sea (ECS) with the South China Sea (SCS) (Figure 1). Chinese mainland and Taiwan Island bound the strait on the west and on the east, respectively. It is about 350 km long, 180 km wide and, on average, 60 m deep [*Chung et al.*, 2001].

[3] Many investigations of volume transport through the Taiwan Strait have been conducted during the last fifty years, since the Taiwan Strait (which is the only channel joining the SCS and the ECS) is very important for water or mass exchange between the SCS and the ECS. Transport through the Taiwan Strait was first touched upon briefly in a report by *Wyrtki* [1961]. His study results indicate that the mean transport is northward along the strait during the period from April to September and southward during the rest of the year. In the recent twenty years, much valuable research has been conducted on this issue. Some results are similar to Wyrtki's in that the seawater generally flows northward in the summer half year and reverses in the winter half year [e.g., *Fang et al.*, 2003; *Wu and Hsin*, 2005], but most studies show that the mean transport direction is northward all year-round and that northward transport is stronger in summer than that in winter [e.g., *Fang et al.*, 1991; *Zilang et al.*, 1991; *Chai et al.*, 2001; *Wang et al.*, 2003]. Generally, direct measurements during hydrographic cruises were limited spatially and discontinuous in time, especially during severe weather when observation ships were often forced to stop surveying. Driving forces used in most numerical models were often from climatological mean values which usually smoothed out the most extreme weather events. As a result, the effects of extreme weather events have not been adequately and reasonably taken into account.

[4] Transport in the strait is not only determined by the oceanic circulation of circumjacent seas and seasonal driving forces, but is also affected by short-term synoptic events. *Ko et al.* [2003] showed that winter wind bursts can induce transport reversals in the Taiwan Strait, which they observed during October and November 1999 using four bottom-mounted acoustic Doppler current profilers laid at four locations across the strait near 25°N. Typhoons are destructive, large-scale atmospheric systems frequently appearing in the area of the Taiwan Strait during summer and autumn. Unfortunately, the influence of typhoons on transport through the Taiwan Strait has been neglected in the literature. Therefore, this study focused on the transport caused by typhoons in the Taiwan Strait hoping to draw attention to the influence of typhoons on transport through the strait.

[5] The remainder of this paper is organized as follows. Section 2 describes the current observations and southward flow events. Section 3 shows the modeling results of transport through the Taiwan Strait, which indicate five strong southward transport events. A numerical model and its validation are also introduced in section 3. Section 4 analyzes the relationship of these southward transport events and the typhoons occurring during the same period. In section 5, three numerical experiments are performed to explain the characteristics of the southward transport events

[1]State Key Laboratory of Marine Environmental Science, Xiamen University, Xiamen, China.
[2]Key Laboratory of Underwater Acoustic Communication and Marine Information Technology of the Minister of Education, Xiamen University, Xiamen, China.
[3]Center for Remote Sensing, College of Marine and Earth Studies, University of Delaware, Newark, Delaware, USA.
[4]School of Marine Sciences, University of Maine at Orono, Orono, Maine, USA.

0148-0227/09/2009JC005372

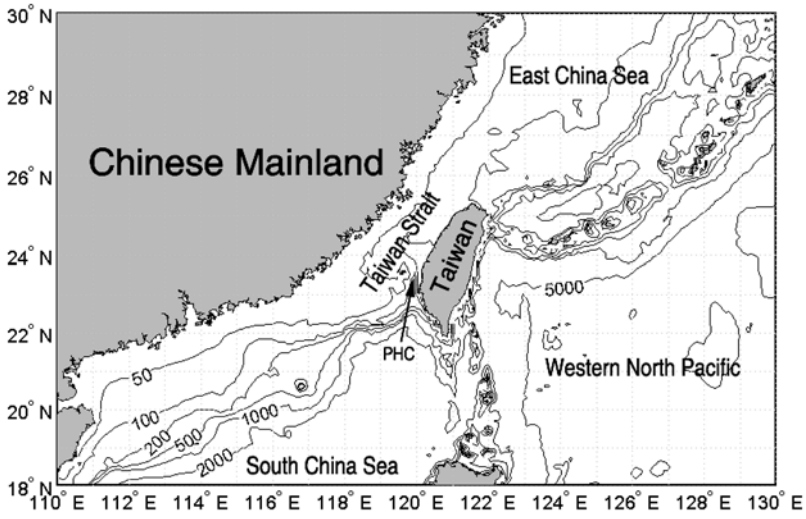

Figure 1. The geographic map and model domain. Depth contours are in m. PHC, Penghu Channel.

due to typhoons, and to examine the effects of the Coriolis force and nonlinear advective terms on the events. The driving factors are discussed in terms of dynamic analysis in section 6, and finally, section 7 presents a conclusion to these results.

2. Current Observations

[6] Measurements of current were very sparse in the Taiwan Strait and there were virtually no direct measurements available during the periods, when typhoons affected the strait, several years ago. Thanks to the implementation of the Chinese Fujian Province Ocean Environment Dynamic, Real-Time, and Three-Dimensional Monitoring System administrated by the Fujian Province Ocean and Fishery Bureau (FOFB), a moored buoy with an acoustic Doppler current profiler and a propeller type wind monitor was deployed in the south middle strait and worked well during the period 25 June 2005 to 22 March 2006 with the exception of a few days of missed observations. Figure 2a shows the locations of the southern section running from west to east via the buoy, and of the northern section. Figure 2b shows the buoy's location in the southern section across the strait. The water depth below the buoy was 66 m compared with the average depth (about 60 m) of the Taiwan Strait. Ten measurement levels were arranged vertically below the buoy at intervals of 5 m with the measurement depth nearest to the sea surface at 5.5 m. The current

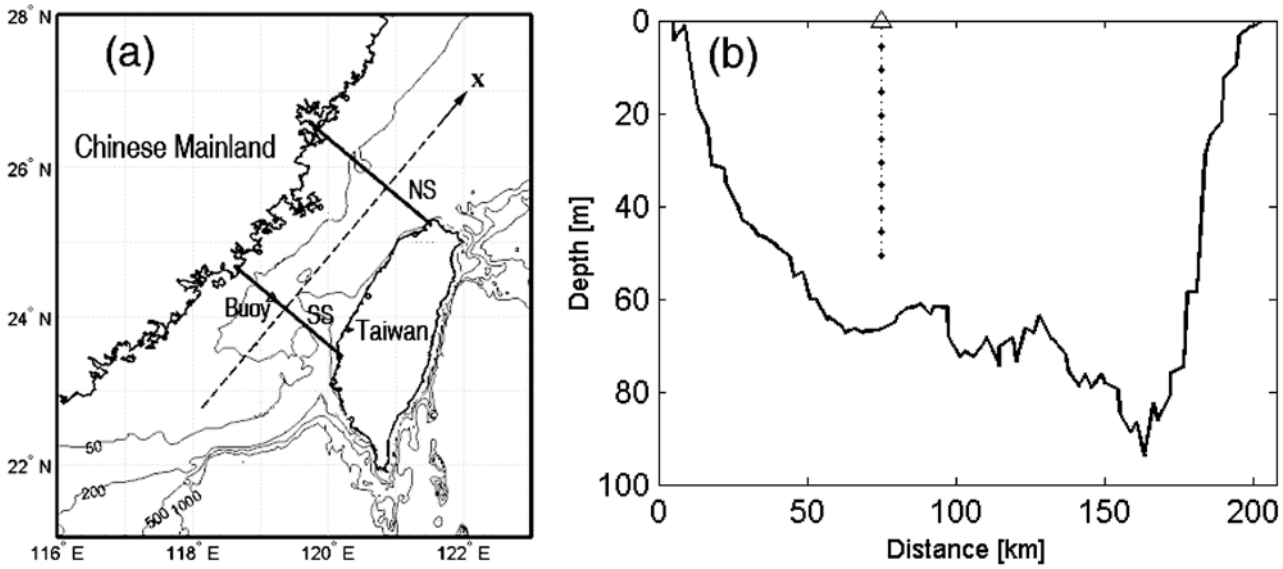

Figure 2. (a) The locations of the sections (denoted by solid lines) and the buoy (denoted by a triangle). SS, southern section via the buoy; NS, northern section in the Taiwan Strait. The dashed line shows the along-strait direction. (b) Current observation levels (denoted by dots) of the buoy in the southern section. The solid line shows the depth along the section from the western bank to the eastern bank of the Taiwan Strait.

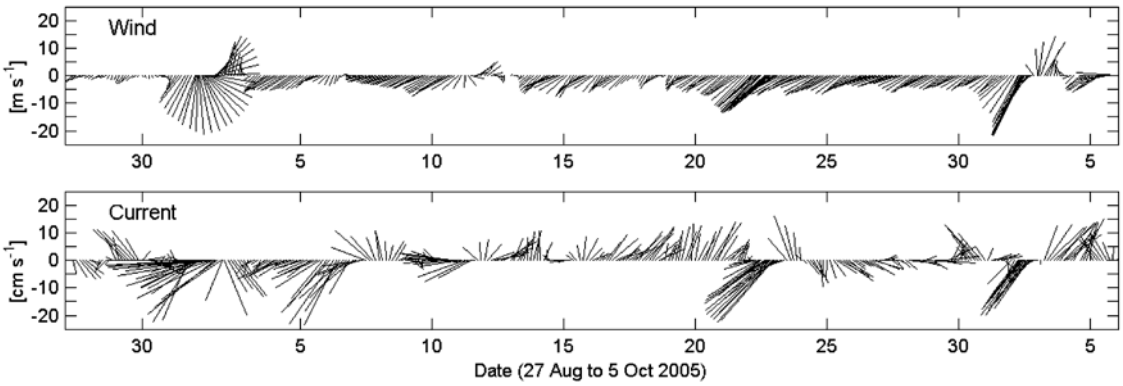

Figure 3. The wind and current data obtained from measurements at the buoy during the period of 27 August to 5 October 2005.

velocities were normally recorded every 3 hours, but sometimes they were measured every hour (mostly during typhoon periods).

[7] At the location of the buoy, the tidal currents were analyzed at every level using the half year data from July to December 2005 via a least squares fit method. Then the tidal current values were removed from the original data. The residual current data during the period of 27 August to 5 October 2005 were used for this study since the monsoon in the study area is weak during this period every year [*Wyrtki*, 1961]. A 25 hour smooth filtering via a nonlinear second power function fit method was performed for the current and wind data in order to remove observational noise. After the above processing, the depth-averaged current and wind data series were obtained from the buoy observations (see Figure 3). There were five typhoons appearing in the western North Pacific Ocean during the period of interest and Figure 4 shows their tracks based on the best track data published by the China Meteorological Administration.

[8] Based on the current data obtained previously, current components along the Taiwan Strait direction could be calculated. The data were interpolated to hourly data via the cubic spline interpolation method to reduce the impact of different sampling temporal spacing on its statistical characteristics. Figure 5 (top) reveals that there were five strong southward flow events which first started to decrease from the mean value (-0.20 cm s^{-1}), then continued to go down beyond one standard deviation (STD) of 10.21 cm s^{-1} and finally increased to end at the mean value. The southward current during each event extended from surface to below 50 m (Figure 5 (bottom)).

3. Modeling Results

3.1. Numerical Model

[9] Since the focus of this study was on transport through the Taiwan Strait, which is a depth-integrated result, the vertical structure of the current and the baroclinic effect are not considered here. A two-way nested coupled tide-surge model (NCTSM) was applied in this study [*Zhang et al.*, 2007]. This model is a two-dimensional barotropic model, based on depth-averaged shallow water equations. Although the model can simulate tide-surge motion, the tides are

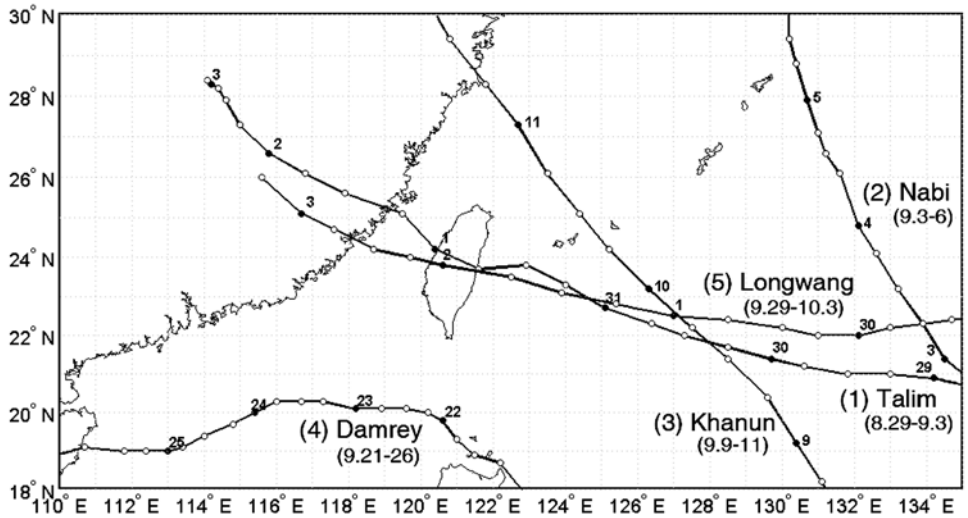

Figure 4. The best tracks of the five typhoons which appeared during the period of 27 August to 5 October 2005. Black dots denote typhoon positions at 0800 local standard time (LST) on the dates labeled by corresponding numbers, white dots denote typhoon positions at 0200, 1400, or 2000 LST.

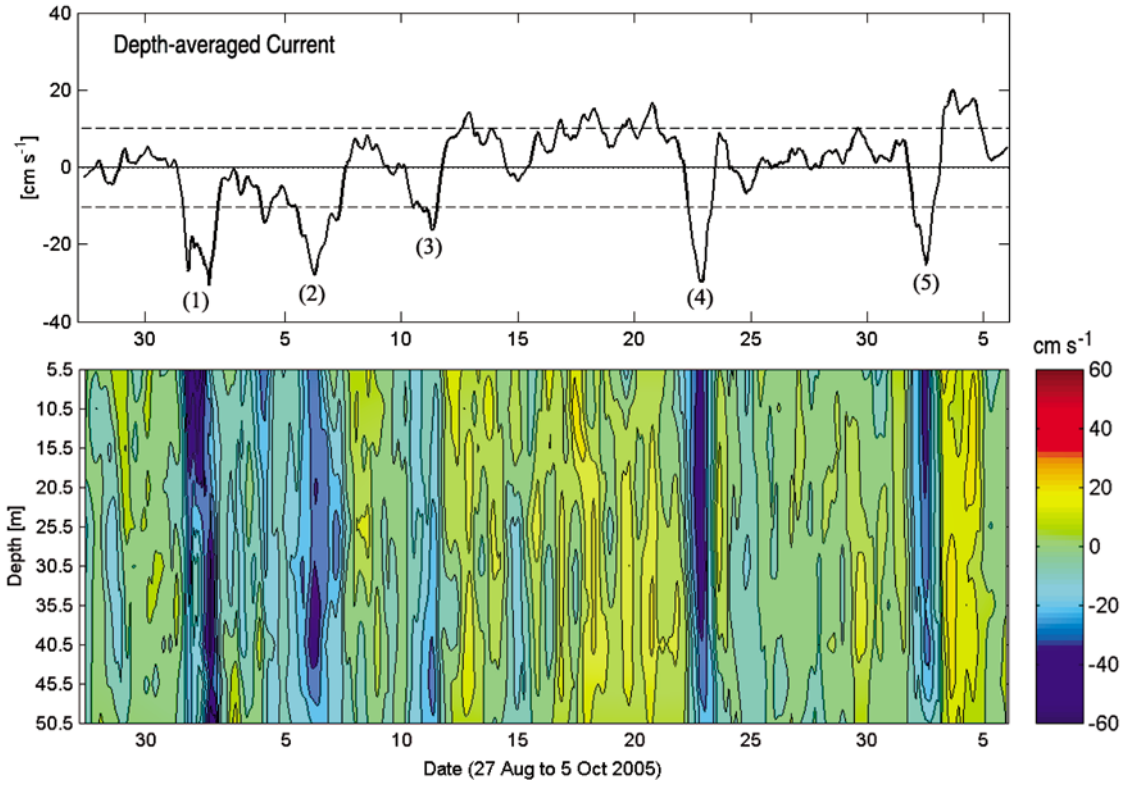

Figure 5. (top) The time series of along-strait depth-averaged current and (bottom) the vertical profile of along-strait current obtained from the buoy observations. In Figure 5 (top), the solid line denotes the along-strait depth-averaged current, the dotted line denotes the mean value, and the dashed lines denote a standard deviation away from the mean value. The numbers in parentheses mark strong southward flow events.

excluded because they are periodic waves and have little influence on the residual flow and on the net transport through the Taiwan Strait.

[10] The model was set up based on the depth-averaged continuity equation and momentum equations in the spherical coordinates. The origin of the system of coordinates was located on the undisturbed sea surface

$$\frac{\partial \zeta}{\partial t} + \frac{1}{R\cos\varphi}\left[\frac{\partial (Hu)}{\partial \lambda} + \frac{\partial (Hv\cos\varphi)}{\partial \varphi}\right] = 0, \tag{1}$$

$$\frac{\partial u}{\partial t} + \frac{u}{R\cos\varphi}\frac{\partial u}{\partial \lambda} + \frac{v}{R}\frac{\partial u}{\partial \varphi} - \frac{uv\tan\varphi}{R} - fv = -\frac{g}{R\cos\varphi}\frac{\partial \zeta}{\partial \lambda} - \frac{1}{\rho R\cos\varphi}\frac{\partial p_a}{\partial \lambda} + \frac{1}{\rho H}(F_s - F_b), \tag{2}$$

$$\frac{\partial v}{\partial t} + \frac{u}{R\cos\varphi}\frac{\partial v}{\partial \lambda} + \frac{v}{R}\frac{\partial v}{\partial \varphi} + \frac{u^2\tan\varphi}{R} + fu = -\frac{g}{R}\frac{\partial \zeta}{\partial \varphi} - \frac{1}{\rho R}\frac{\partial p_a}{\partial \varphi} + \frac{1}{\rho H}(G_s - G_b), \tag{3}$$

where the notations are as follows:

t time;
λ, φ east longitude and north latitude;
ζ sea surface elevation above the undisturbed sea level (above which it is positive and below which it is negative);
h depth of undisturbed water;
H total water depth, $H = h + \zeta$;
u, v east and north components of the depth-averaged current, **q;**
F_s, G_s components of the wind stress on the sea surface, $\boldsymbol{\tau}_s$;
F_b, G_b components of the bottom stress, $\boldsymbol{\tau}_b$;
p_a atmospheric pressure on the sea surface;
R radius of the earth;
g acceleration due to gravity;
f Coriolis parameter, $f = 2\omega\sin\varphi$, here ω is the angular speed of the earth's rotation;
ρ density of seawater, assumed to be unchanged.

[11] The following quadratic law, widely used in the literature, was applied in the bottom friction parameterization:

$$\boldsymbol{\tau}_b = \rho g c^{-2}|\mathbf{q}|\mathbf{q}, \tag{4}$$

where c is the Chezy coefficient; $c = H^{1/6}/n$ (n denoting the Manning coefficient). The parameterization of the wind stress was also completed with a quadratic law as follows:

$$\boldsymbol{\tau}_s = \rho_a C_d|\mathbf{W}|\mathbf{W}, \tag{5}$$

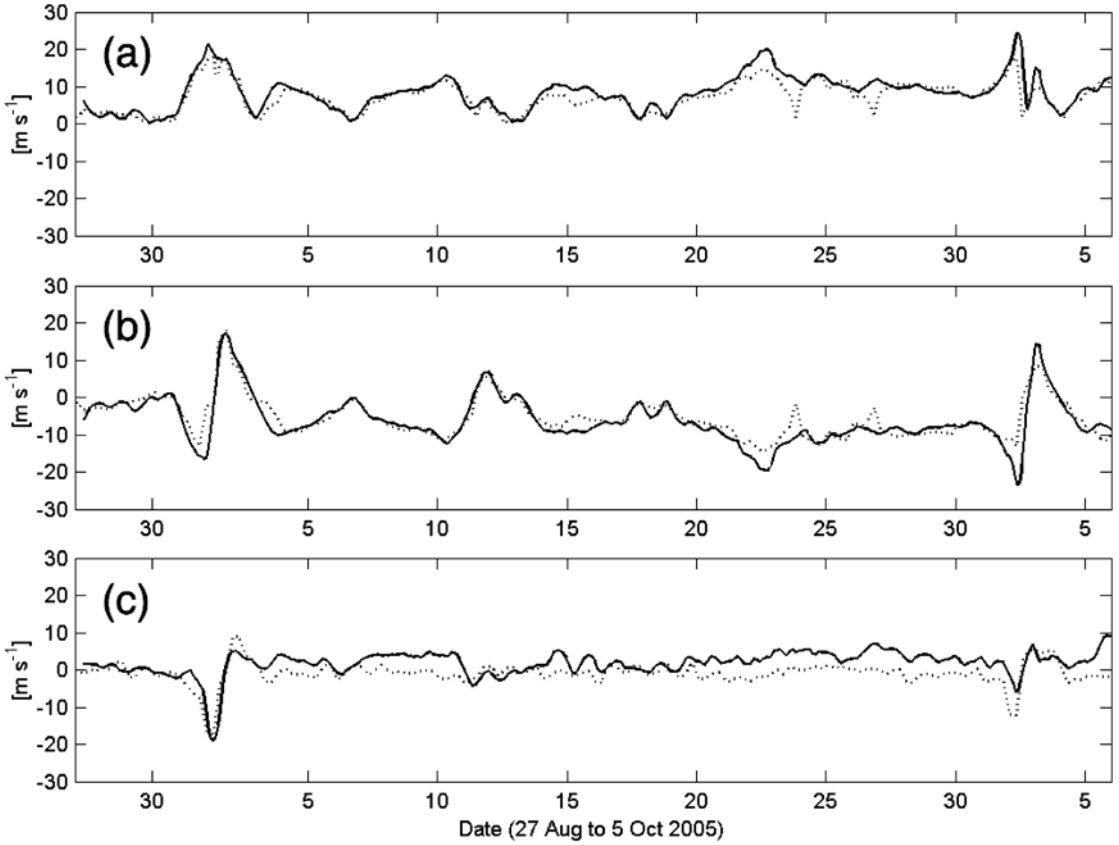

Figure 6. A comparison between the wind observations at the buoy (solid lines) and the blended wind data (dotted lines). (a) The total wind speed, (b) the along-strait component, and (c) the across-strait component.

where C_d is the wind stress coefficient; ρ_a the density of air; and **W** the wind vector at a height of 10 m above sea surface. C_d is determined from this equation [*Zhang et al.*, 2007]

$$C_d \times 10^3 = \begin{cases} 1.052, & |\mathbf{W}| \le 6\ \mathrm{m\,s^{-1}} \\ 0.638 + 0.069|\mathbf{W}|, & 6 < |\mathbf{W}| < 30\ \mathrm{m\,s^{-1}} \\ 2.708, & |\mathbf{W}| \ge 30\ \mathrm{m\,s^{-1}} \end{cases}. \quad (6)$$

[12] The model domain is shown in Figure 1. The coarse grid mesh (110∼130°E, 18∼30°N) of the model has a resolution of 1/10° (about 11.1 km) and the fine mesh (113.3∼121.5°E, 22.0∼28.4°N) has a resolution of 1/30° (about 3.7 km). Along the coastal boundaries, no water was allowed to flow through, which means that the normal component of the current vanished. On the open boundaries, a radiation condition was used as follows:

$$q_n = \hat{q}_n \pm \frac{C}{H}\left(\zeta - \hat{\zeta}\right),\ C = \sqrt{gH}, \quad (7)$$

where the subscript n stands for the component normal to the open boundary, and $\hat{\zeta}$ and $\hat{q}_n$ are the water level input and current input on the open boundary, respectively, which can be prescribed beforehand or be determined by local solution [*Zhang et al.*, 2007]. More details about the NCTSM are given by *Zhang* [2006] and *Zhang et al.* [2007].

3.2. Driving Forces

[13] The meteorological driving forces include wind stress and atmospheric pressure gradient, and the wind field and pressure field above the sea surface are necessary to calculate the wind stress and the pressure gradient, respectively. The wind fields we adopted were blended 6 hourly wind fields gridded in a 0.25° geographical grid which were derived by merging the remotely sensed wind observations and the operational ECMWF wind analyses (referred to as the blended wind hereafter). The remotely sensed wind observations were retrieved from the Seawinds scattermeter onboard the QuikSCAT satellite and from the Special Sensor Microwave Imager onboard the Defense Meteorological Satellites Program satellites F13, F14 and F15. To our best knowledge, this blended wind data set is the finest horizontal spatial resolution surface wind data set over the global oceans up to the present. The blended wind data compared well with remotely sensed wind observations and buoy estimates (see http://cersat.ifremer.fr/layout/set/print/data/discovery/by_product_type/gridded_products/mwf_blended and ftp://ftp.ifremer.fr/ifremer/cersat/products/gridded/mwf-blended/documentation/BlendedWind-Doc_27112006.pdf). The correlation coefficients (*Rs*) between the blended wind data and the remotely sensed wind observations exceed 0.95 while the root-mean-square (RMS) difference values are less than 0.30 m s^{-1}. The

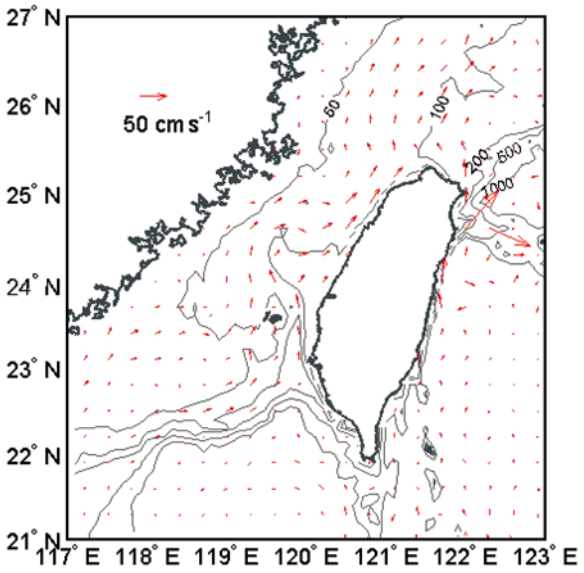

Figure 7. The simulated mean depth-averaged circulation pattern during the period of 27 August to 5 October 2005. The gray lines are depth contours in m.

wind speed *Rs* between the blended wind data and the buoy estimates range from 0.80 to 0.90 and the RMS difference values are less than 2 m s^{-1}. Figure 6 shows a comparison between observations performed at the buoy in the Taiwan Strait and the blended wind data. The *R* between their wind speeds (952 pairs of data) was 0.90 and the RMS difference value was 2.3 m s^{-1}. For along-strait components, the *R* was 0.91 and the RMS difference was 2.64 m s^{-1} while for across-strait components, they were 0.62 and 3.80 m s^{-1}, respectively. The mean wind speed of the blended wind data was 0.97 m s^{-1} smaller than that of the buoy observations based on the original 6 hourly data. Generally speaking, the blended wind data also compared well with the buoy observations in this region although wind speeds were slightly underestimated by the blended data, and along-strait components showed better comparisons than across-strait components.

[14] The surface air pressure fields were from the 6 hourly global surface pressure data set performed by the NCEP/NCAR Reanalysis 1 project, which uses a state-of-the-art analysis/forecast system to perform data assimilation using past data from 1948 to the present. This data set has a spatial resolution of 2.5° latitude and 2.5° longitude and a temporal spacing of 6 hours.

[15] The impact of ocean circulation and meteorological driving forces out of the model domain on the current in the model domain was taken into account by momentum input on the open boundary. The momentum input on the open boundary was implemented by providing the across-boundary current component for the boundary condition as its preceding current. The currents on the open boundary were taken from the 5 daily ocean reanalysis data set of the NCEP Global Ocean Data Assimilation System, which has a resolution of 0.33° latitude and 1.00° longitude and 40 levels in the vertical direction. We interpolated 40 levels of data into every meter level via the spline interpolation method and then computed their mean values as depth-averaged currents. The wind field, the air pressure field and the depth-averaged current data (as noted above) were spatially interpolated to NCTSM grids via two-dimensional bicubic interpolation method and temporally interpolated to every time step via linear interpolation.

3.3. Current Simulation and Validation

[16] Using the NCTSM and the driving forces mentioned above, we simulated the current in the Taiwan Strait during the period of 27 August to 5 October 2005. The numerical model was first driven for 6 months using the monthly atmospheric data and current data of July 2005 until the simulation results were not changed perceptibly during the past day, and then it was driven by the 6 hourly atmospheric data and 5 daily current data from 26 July to 6 October 2005. The hourly modeling results during the period of 27 August to 5 October 2005 were compared with the buoy observations as described previously. The RMS difference value between model results and buoy observations was 6.28 cm s^{-1} in current velocity and 36° in current direction with a current velocity over 20 cm s^{-1}. The modeling results were generally in good agreement with buoy observations.

[17] Figure 7 shows the simulated mean depth-averaged current during the period of 27 August to 5 October 2005. This depth-averaged circulation pattern in early autumn was similar to that of fall presented by *Jan et al.* [2002] and *Wu et al.* [2007] except for the absence of weak China coastal current in the northwestern part of the Taiwan Strait. September is the transition period from southwest monsoon to northeast monsoon when the northeast winds begin to occur in some local regions and the south monsoon loses only slightly in strength in the other parts of Asia [*Wyrtki*, 1961; *Jan and Chao*, 2003]. *Wyrtki* [1961] indicated that the monsoon current of the south monsoon season decays by the end of September and at that time the current of the north monsoon season is not yet established. The absence of the China coastal current induced by the northeast monsoon was conceivable during the period. A northward current is obvious at the Penghu Channel in Figure 7, which is consistent with *Jan and Chao*'s [2003] results obtained from the current measurements using the shipboard Acoustic Doppler Current Profiler during 1999–2000. On the shelf north of the Taiwan Island, the circulation pattern shows the onshore intrusion of Kuroshio. Similar onshore intrusion of Kuroshio can also be found in the numerical results and the current measurements at a depth of 20 m both in summer and in winter given by *Fang et al.* [2001] and *Tang et al.* [2000], respectively. Therefore, the simulated mean circulation pattern was reasonable, indicating that the numerical model basically worked well in the Taiwan Strait.

3.4. Transport Through the Taiwan Strait

[18] Transports through the northern section and the southern section were calculated using the data output by the NCTSM. Figure 8 shows that the transport series through these two sections varied synchronously and the two curves were almost coincident, indicating that transport was through the entire strait. For this reason, only the transport through the southern section will be considered hereafter. The mean transport during this period was 0.35 Sv, which is almost the same as the results for September of 1999–2003 simulated by *Wu and Hsin* [2005] using the East Asian Marginal Seas model driven by 6 hourly blended QSCAT/

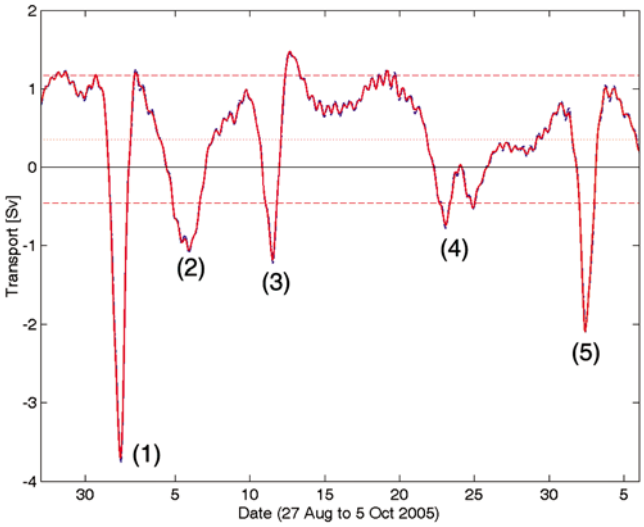

Figure 8. Time series of transport through the southern section (red line) and the northern section (blue line). Northward transport is positive and southward transport negative. The solid lines denote transport series, the dotted line denotes the mean value, and the dashed lines denote a standard deviation away from the mean value. The numbers in parentheses mark the strong southward transport events.

NCEP wind stress, but is remarkably smaller than the result of 2.01 Sv in September simulated by *Chai et al.* [2001] using the Princeton Ocean Model forced by climatological monthly mean winds. The STD of the transport during this period was 0.81 Sv. It can be seen also that there were five strong southward transport events with their amplitudes exceeding one STD from the mean transport. The five southward transport events were consistent with the five southward flow events mentioned previously.

[19] *Wu and Hsin* [2005] set up a statistical relationship between transport through the Taiwan Strait and along-strait wind stress obtained by averaging the QSCAT wind stress in the domain from 118°E to 120°E and from 23°N to 25°N, which can be written in the form

$$Q = 10.6 \times WS + 1.99, \tag{8}$$

where Q is the transport (Sv) and WS is the along-strait wind stress (N m^{-2}). Using this equation, we calculated the transport through the Taiwan Strait based on the blended wind data in the same domain. The results are shown in Figure 9 after their mean value was removed. Although the blended wind data differed from the data set used by *Wu and Hsin* [2005], the difference was negligible since the blended wind data compared well with the QSCAT wind observations as mentioned previously. The results basically reflected the variations of transport simulated by the numerical model. There was still some difference existing between its results and the modeling results. As seen from Figure 9, the transport calculated by equation (8) leads the modeling results, which is caused for the same reason that the wind leads the current in the Taiwan Strait [*Chuang*, 1985]. *Chuang* [1985] explained that a frictional adjustment time is required for the water to reach a certain speed at which bottom stress balances the wind stress or the energy input from the wind is working to accelerate the fluid during this period of time. An unordinary northward transport appeared in the results given by equation (8) on 2–3 September, when the strong southwestward wind changed to a strong northeastward wind and then the wind speed decreased rapidly (Figure 3). Actually, the strong northeastward wind must hurdle the strong southward flow before it induces a northward transport. The numerical results did not show this strong northward transport (Figure 9) because the northeastward wind did not persist for enough time to reverse southward current (see Figure 3). The transport series given by equation (8), which only depended on the local wind stress, missed the southward transport event 2 since the local wind was weak during the period of 5 to 7 September.

[20] Based on the transport data derived from the simulation results output by the model and the along-strait current data at the location of the buoy during the period of 27 August to 5 October 2005, we obtained a statistical relationship between transport through the Taiwan Strait and the along-strait current at the buoy location (Figure 10), which can be described by the equation

$$Q = 0.0842U + 0.1, \tag{9}$$

where U (cm s^{-1}) is the current component normal to the southern section, namely along-strait current, at the location of the buoy. The R between the along-strait current and the transport was 0.95 with a corresponding statistical significance of 99%. Now we could calculate the transport via equation (9) using the current observations at the buoy. For comparison, the results after removing the mean value are shown in Figure 9. The results were in good agreement with the modeling results. Compared with the modeling results, there was no significant and systemic time shift. Seen from Figure 9, the equation (9) underestimates the southward transport event 1 and overestimates the events 2 and 4. All

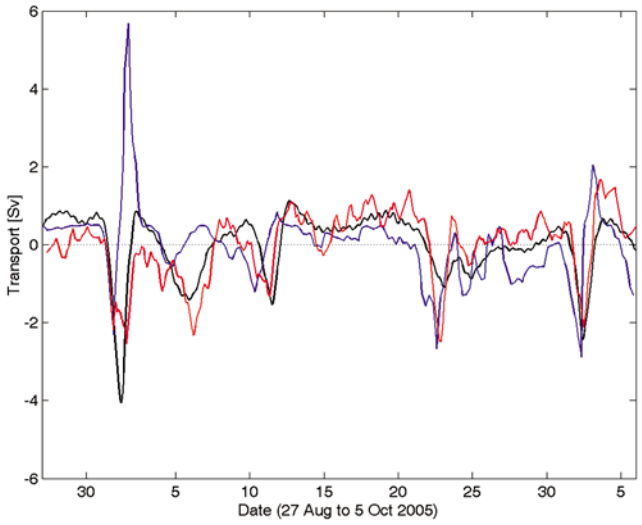

Figure 9. Comparison of the transport time series obtained using three different methods: numerical model simulations (black line), results calculated from the wind data set (blue line), and results calculated from the buoy current observations (red line).

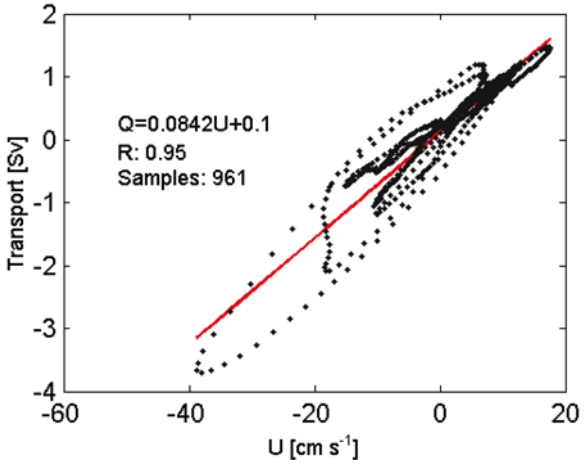

Figure 10. The transport through the southern section versus the depth-averaged currents at the location of the buoy, based on the data output from the model. The solid red line is the fitted line.

the transport results obtained by the above three methods demonstrated five strong southward transport events, except that the second event was missed by the method based on equation (8) due to weak local wind.

4. Relationship Between Southward Transport Events and Typhoons

[21] The five southward transport events coincided with the activities of the five typhoon events which occurred in the western North Pacific during the same period, as can be seen from Figures 8 and 4. Typhoon Talim in 2005 was a typical typhoon affecting the Taiwan Strait. It basically moved northwestward and traversed the strait. The wind, observed at the buoy, rotated in an anticlockwise manner changing from southwestward to northeastward as the typhoon passed the strait (Figure 3). The strong southward wind caused the water to flow southward since the typhoon moved close to the strait on 31 August (Figure 11a), which led to a strong southward transport in the strait (event 1 in Figure 8). The southward transport weakened after the typhoon landed and ended on 2 September. Typhoon Longwang in 2005 was another typical typhoon and seemed to move generally westward. The southwestward wind due to the typhoon became stronger as the typhoon came nearer to the buoy. The southwestward wind abruptly stopped and then the wind direction turned northwestward and rotated clockwise as the typhoon passed the buoy. At the same time, the current was directed southwestward before the typhoon arrived in the region of the buoy and almost reversed after the typhoon landed at the mainland coast (Figures 3 and 11b). Figure 8 shows that the transport was northward during the period of 26 to 30 September although the southwestward wind prevailed during this period (see Figure 3). When the southwestward wind strengthened due to Longwang, the transport turned south swiftly and gradually became stronger. It reached its southward maximum of 2.1 Sv when the typhoon came closest to the buoy, and then decreased with the wind turning northward when the typhoon left the buoy region. Consequently, a similar southward transport event took place due to Typhoon Longwang (event 5 in Figure 8).

[22] Although Typhoon Damrey in 2005 moved westward in the northern SCS, it obviously enhanced the local southwestward wind in the Taiwan Strait (Figure 3) when it came close to the strait. The enhanced wind forced the northeastward current to reverse (Figures 3 and 12a), which resulted in southward transport through the Taiwan Strait (event 4 in Figure 8). The southward transport reached its maximum of 0.7 Sv when the typhoon was nearest to the strait. After that, the southwestward wind in the strait weakened and the current flowed northward again with its direction rotating clockwise. Subsequently, the southward transport ended. Similarly, the weaker Typhoon Khanun in 2005 also produced a southward transport event (event 3 in Figures 8 and 12b) in the Taiwan Strait when it quickly moved over the sea area north of the strait.

[23] Typhoon Nabi in 2005 was very far away from the Taiwan Strait for its whole lifetime. However, an unexpected southward transport event happened in the Taiwan Strait during this typhoon (event 2 in Figure 8). It can be seen from Figures 3 and 4 that the southwest current began on 3 September and gradually increased until 6 September when Nabi came near to the strait. Although the southwest current was underestimated by the numerical model, it was still perceptible in Figure 13. Subsequently, the flow decreased and then turned northward, as in the previous two events. It was different from the other events since the southwestward wind was very weak during this event, indicating that the local wind here was not the main reason for this southward transport event. This could be validated by the fact that the along-strait current velocity in the surface layer (<10.5 m) was smaller than that in the middle layer (30.5∼40.5 m) during this event (Figure 5). If the local wind was the main driving force of current, then the current velocity of the upper layer would be larger than that of the lower layer. Nabi was very strong with a minimum center pressure of 920 hPa and a maximum wind of 60 m s^{-1}, and its scale was so large that the wind scope of over 7 on the Beaufort scale had a radius of 650 km on 5 September. The strong outer southward winds of Nabi covered the continental shelf sea area of the ECS north of the Taiwan Strait, which could be confirmed using QuikSCAT remotely sensed wind data on 5 September (Figure 14). This data showed very strong southward winds with speeds over 15 m s^{-1} in the sea area north and northeast of Taiwan Island while the winds in the Taiwan Strait were weak with speeds under 10 m s^{-1}. It is a possible mechanism that the remote wind forcing of Nabi could produce the southward transport event in the Taiwan Strait.

5. Numerical Experiments

[24] In order to obtain the characteristics of the southward transport events due to typhoons and analyze the influences of the Coriolis force as well as the nonlinear advective term on the southward transport through the Taiwan Strait, we conducted three idealized numerical experiments using the NCTSM. For simplicity and generality, we used four synthetic typhoons and adopted a widely used analytic axisymmetric wind model [*Holland*, 1980] with an empir-

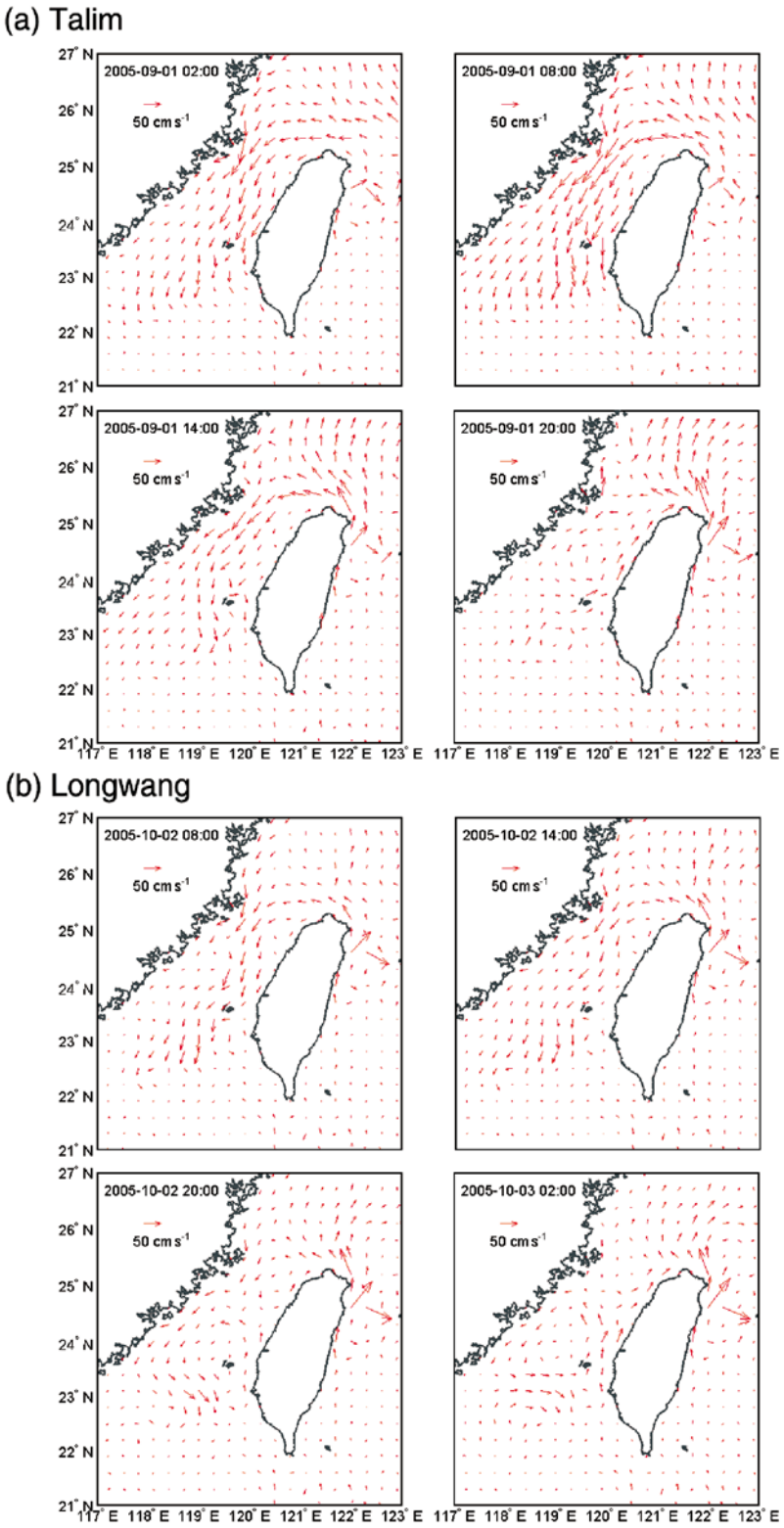

Figure 11. Circulation variation in the Taiwan Strait during typhoons (a) Talim and (b) Longwang.

ical moving wind field model [*Jelesnianski*, 1965] and an analytic axisymmetric air pressure model [*Holland*, 1980] to describe the wind and air pressure fields of the synthetic typhoons. The seasonal circulation and the effects of the terrain over Taiwan Island on the wind and air pressure fields were not considered here for the same reason. Our modeling results (not shown here) showed that the northward seasonal circulation in the Taiwan Strait could reduce

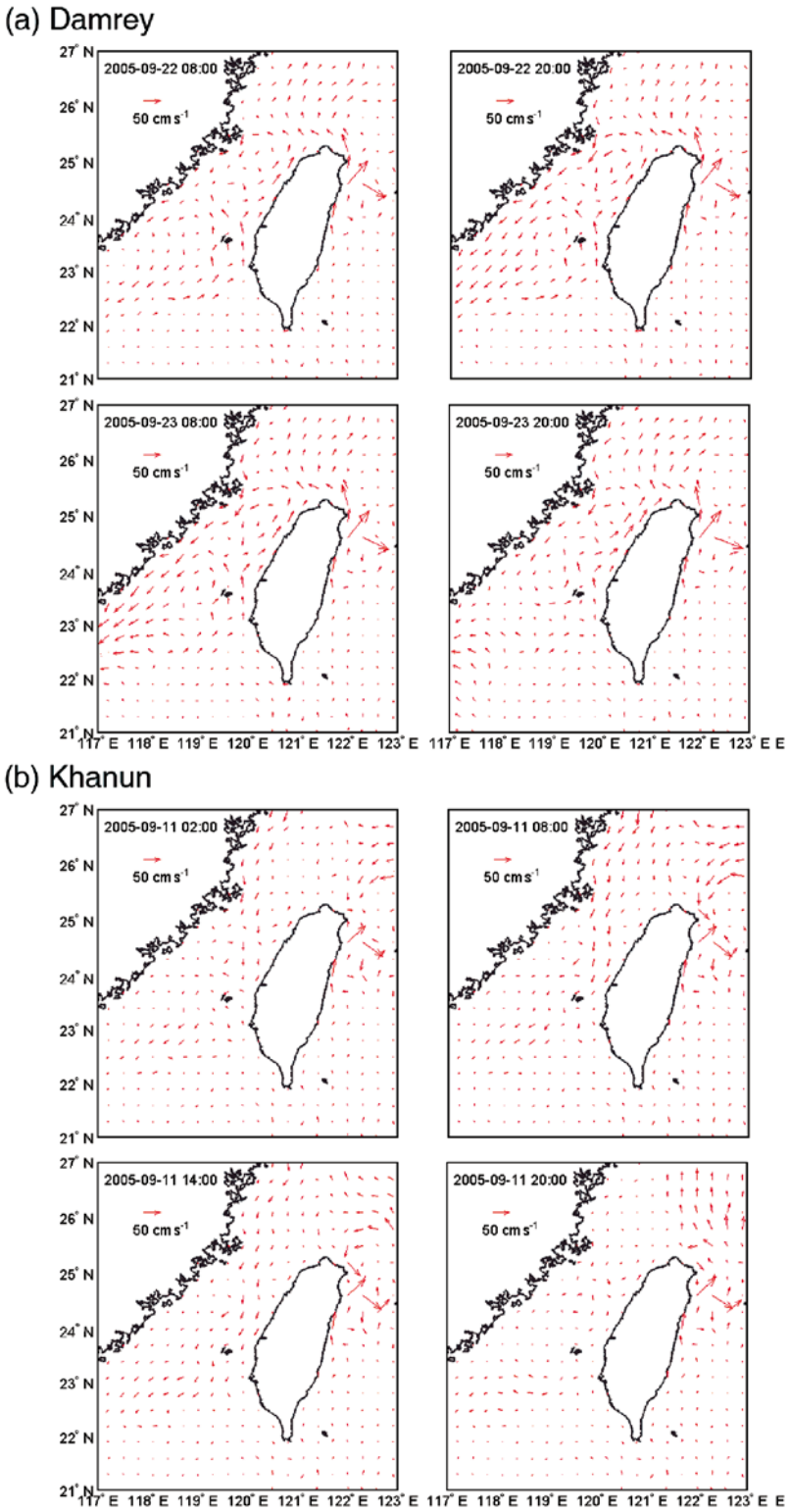

Figure 12. Circulation variation in the Taiwan Strait during typhoons (a) Damrey and (b) Khanun.

the intensity of the southward transport event due to a typhoon, but it did not prevent this event from happening.

[25] These synthetic typhoons were moderately strong with a maximum wind speed of 35 m s^{-1} and a lowest central pressure of 970 hPa. They moved northwestward at a speed of 20 km h^{-1} along four different routes, which were representative of the most common routes of typhoons affecting the Taiwan Strait (Figure 15). Additionally, the four typhoons provided different dynamical influence on the Taiwan Strait, since the strait is located at dissimilar quad-

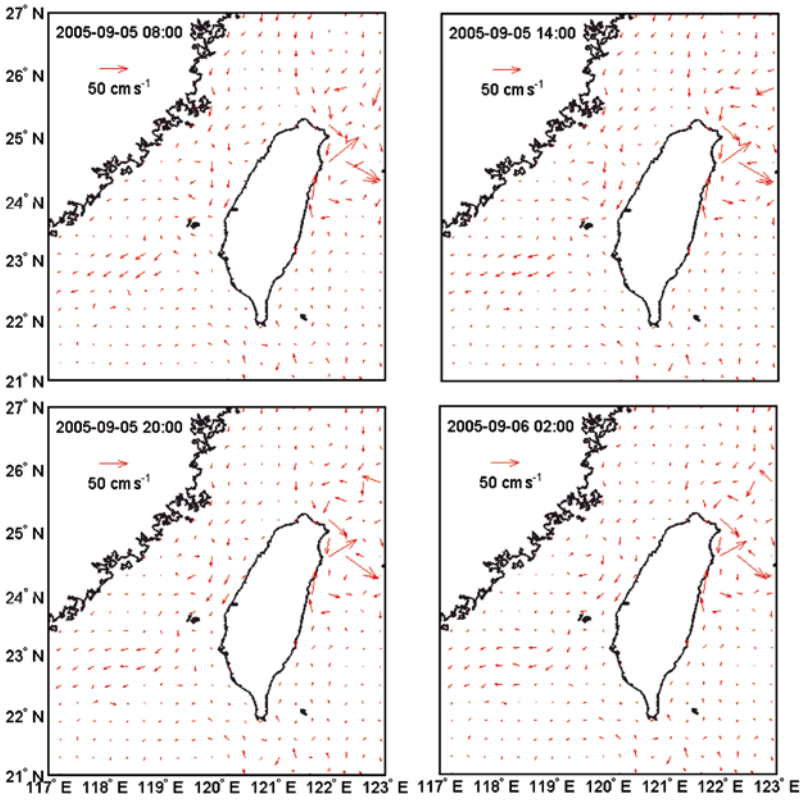

Figure 13. Circulation variation in the Taiwan Strait during Typhoon Nabi.

rants from the typhoons. The Taiwan Strait lies on the left (right) side of the first (fourth) synthetic typhoon, where the wind direction is backward (toward) the mainland. The second and the third typhoons passed through the northern and the southern part of the Taiwan Strait, respectively.

[26] The first experiment was to simulate the transport variations in the Taiwan Strait due to the four synthetic typhoons. Figure 16 shows that transport through the southern section induced by the four synthetic typhoons was southward and each of them displayed a southward transport event. When a typhoon came near to the Taiwan Strait, the transport began to direct southward and its amplitude increased gradually. The southward transport reached its maximum value before the typhoon landed on the coast of Chinese mainland. Subsequently, its amplitude began to decrease and finally the southward transport vanished when the typhoon moved away from the Taiwan Strait. It should be noted that after the typhoon landed at the coast, the transport was not directed northward immediately and no evident northward transport event appeared although a strong northward wind existed in the Taiwan Strait behind the typhoon's center. This was because the energy input from the northward wind was depleted to attenuate the southward movement of the seawater. Therefore the effect of a typhoon on transport through the strait appeared to be a horizontal "pumping" effect, pumping seawater into the SCS from the ECS.

[27] In the second experiment, the Coriolis force was omitted while the other aspects were the same as in the first experiment. The results showed that southward transport without the Coriolis force was stronger than with the Coriolis force in all four cases (Figure 16), indicating that the Coriolis force made a negative contribution to these southward transport events.

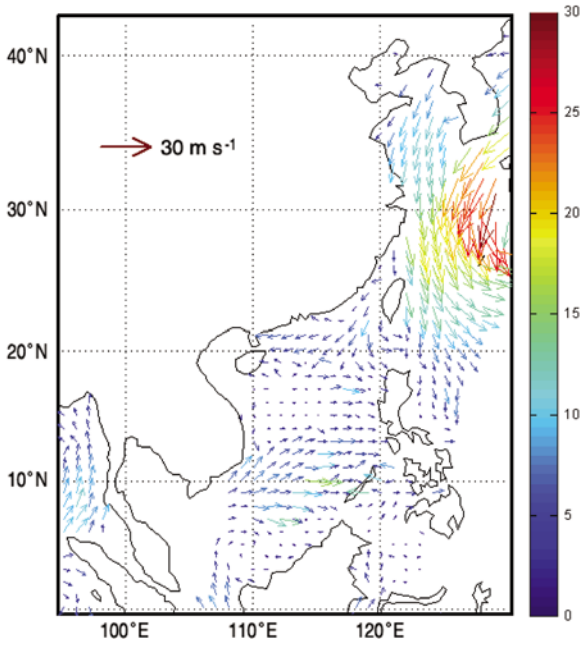

Figure 14. Wind field observed by QuikSCAT on 5 September 2005. Both the length and color of the arrow show the wind speed (m s^{-1}).

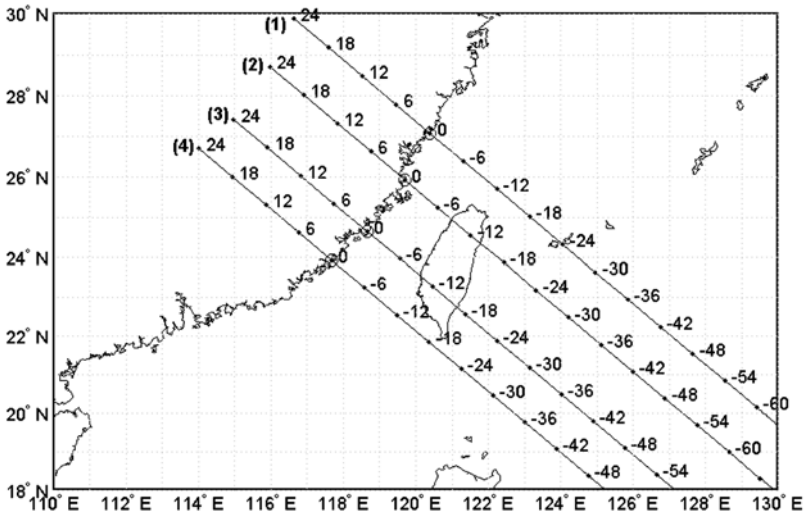

Figure 15. The tracks of the four synthetic typhoons. The numbers are the hours before (negative) or after (positive) the landing time of the typhoon.

[28] The third experiment involved the absence of nonlinear advective terms and was performed to evaluate the influence of nonlinear advective terms on southward transport events in the Taiwan Strait. The results were almost the same as those of the first experiment (Figure 16), demonstrating that advective terms had little effect on southward transport events.

6. Dynamic Analysis

[29] In order to analyze the driving factors for the southward transport events, we obtained the following along-strait transport equation (10) based on the momentum equation in the along-strait direction and the continuity equation in the two-dimensional Cartesian coordinates. The detailed derivation of this equation is given in Appendix A

$$\frac{\partial Q}{\partial t} = -\frac{\partial}{\partial x}\int_{-b/2}^{b/2} HU^2 dy - \int_{-b/2}^{b/2}\left(C^2\frac{\partial \zeta}{\partial x}\right)dy + \int_{-b/2}^{b/2}\frac{F}{\rho}dy + \int_{-b/2}^{b/2} fHV dy, \tag{10}$$

where F is the combination of external compelling forces (wind stress, air pressure gradient force and bottom stress);

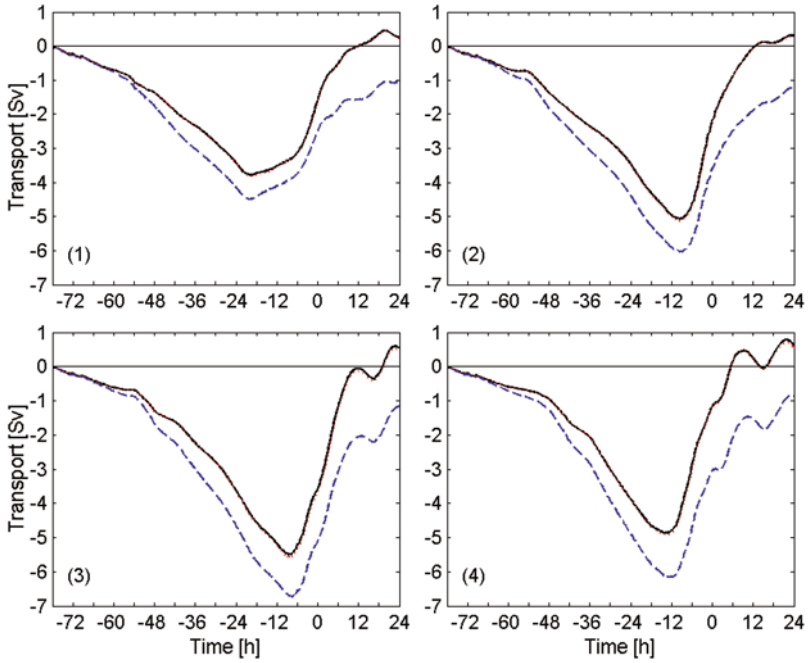

Figure 16. Transport through the Taiwan Strait due to the four synthetic typhoons. Black solid lines show the transport simulated by the model, dashed lines denote the results without Coriolis forces, and dotted lines denote the results without nonlinear advective terms. The numbers on the transverse axis are the hours before (negative) or after (positive) the landing time of a typhoon.

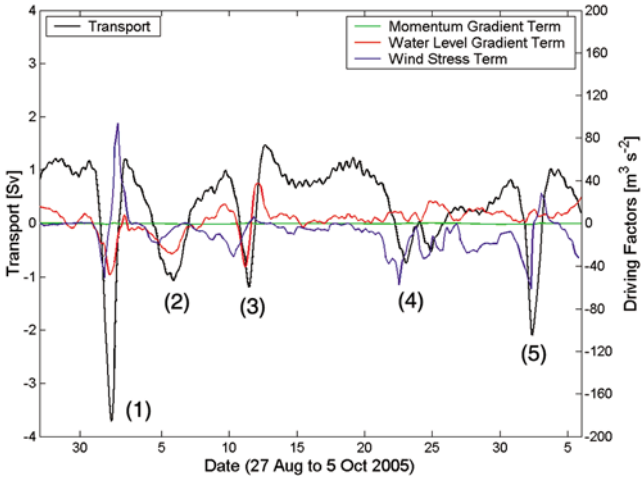

Figure 17. Time series of transport (black line), momentum gradient term (green line), water level gradient term (red line), and wind stress term (blue line) during the period of 27 August to 5 October 2005.

U and V are the along-strait and across-strait depth-averaged current components, respectively; b denotes the width of the Taiwan Strait and $C = \sqrt{gH}$. The last term on the right-hand side of equation (10) is related to the Coriolis force which has a negative contribution to the transport events as described in the previous numerical experiments. *Allen and Kundu* [1978] found from current measurements that the alongshore components of both local acceleration and Coriolis force are remarkably negatively correlated on the continental shelf off Oregon, which is consistent with our result of numerical experiments in the Taiwan Strait. Therefore, the possible driving factors of the southward transport events are the three terms on the right-hand side of the above equation. The first of these terms is the along-strait momentum gradient (originated from the advective term) in the Taiwan Strait, which provides net momentum input between the northern and southern ends of the strait; the second is related to the water level gradient in the along-strait direction, reflecting the forcing effect of pressure gradient force; and the third is the function of local forces among which the main driving force is wind stress in the shallow waters.

[30] Figure 17 shows the variations in the first term, the second term and the wind stress term. The first and the second terms were calculated from the data for the southern section and the northern section output by the numerical model, and the wind stress term was based on the blended wind data set in the domain from 118°E to 120°E and from 23°N to 25°N. It is very clear that the momentum gradient term was quite negligible compared with the other two terms. Actually, the dimensional analysis also showed that this term was smaller by at least 2 orders than the second term. The second term was comparable to the wind stress term. The wind stress term led the transport for several hours, which is consistent with *Chuang*'s [1985] results. There was little time lag between the water level gradient term and transport, indicating that the current adjusted very quickly to the water level gradient in the Taiwan Strait. The wind stress term here included only the local wind effect. The along-strait water level gradient in the Taiwan Strait could be developed by the uneven distribution of storm surges caused by typhoons. The storm surge is generated by wind stress (wind setup) and air pressure gradient force. In shallow water, wind stress is the main forcing factor of storm surges.

[31] It can be seen from Figure 17 that the combination of water level gradient and local wind stress resulted in the southward transport event 1 due to Typhoon Talim. The magnitude of water level gradient term was comparable with that of wind stress term. The southward transport event 5 due to Typhoon Longwang was mainly induced by local wind stress. The influence of water level gradient was insignificant. Typhoons Talim and Longwang had a similar track, moving westward and traversing the Taiwan Strait, but there was some difference between them. Talim moved across the northern part of the strait while Longwang moved across the southern part. Additionally, the former had a larger scope with a radius of 450 km over 7 on the Beaufort scale than that of the latter with a corresponding radius of 350 km when they entered the Taiwan Strait. The direct result of these differences was that there was stronger shoreward wind in the sea area north of the Taiwan Strait during Talim than that during Longwang, which could be easily confirmed by QuikSCAT remotely sensed data (the figure omitted). The indirect result was that higher storm surge elevation due to stronger shoreward wind appeared in the northern sea area of the Taiwan Strait during Talim than that during Longwang (see Figures 18a and 18b). It can be seen that the along-strait water level gradient between the two sections was significant in Figure 18a while it was insignificant in Figure 18b, which is consistent with the results in Figure 17. Therefore, the southward transport events 1 and 5 had some different dynamic mechanism although the tracks of typhoons Talim and Longwang looked alike.

[32] It was noted that there were no strong northward transport events appearing after typhoons Talim and Longwang landed on the mainland coast although the winds in the Taiwan Strait turned northward. A static typhoon in the open sea is basically an axisymmetric circular system. When it moves along a track, its right side seen in the direction of motion has a higher wind speed than the left side [*Jelesnianski*, 1965]. Typhoon usually becomes weak after it lands with its energy decreasing due to the bottom friction of land. The wind speed around its center lowers. Accordingly, the southward wind, as typhoon comes closer to the Taiwan Strait, is stronger than the northward wind, as typhoon leaves the strait. At the same time, the southward current velocity induced by the stronger southward wind must be larger than the northward current velocity induced by the northward wind, which can be seen in Figure 3 during Typhoon Longwang as an example. Even if the typhoon does not become weak after it lands, the northward wind must first overcome the inertial motion of southward flow induced by the preceding southward wind before it sets up a northward current. For this reason, a remarkable northward transport is hard to be induced by the northward wind behind the typhoon center in the Taiwan Strait, which

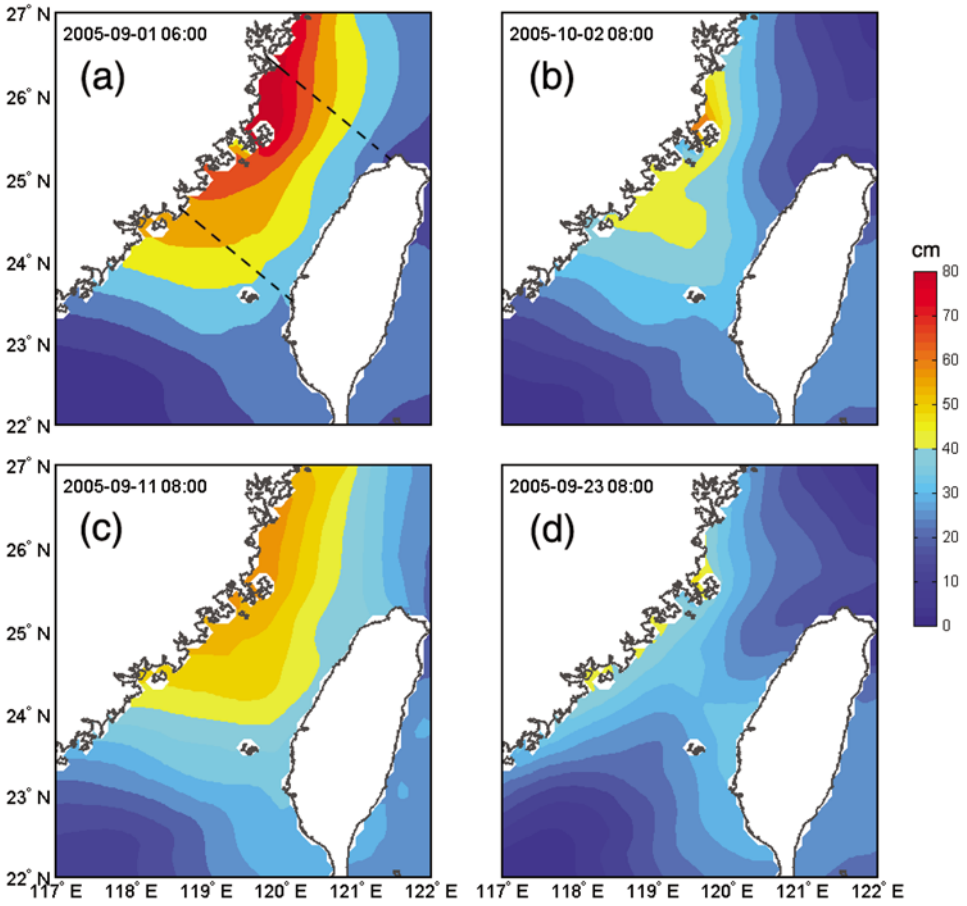

Figure 18. The water level patterns induced by typhoons (a) Talim, (b) Longwang, (c) Khanun, and (d) Damrey. The black dashed lines show the positions of the two sections mentioned in Figure 2a.

has been confirmed by the numerical experiments described previously. Therefore, the net transports during Talim and Longwang were southward.

[33] During typhoons Khanun and Nabi, the local wind in the Taiwan Strait was weak (Figure 3) and the magnitude of the wind stress term was smaller than that of the along-strait water level gradient term (Figure 17). The southward transport events 2 and 3 due to these two typhoons were caused mainly by the along-strait water level gradient term. Both typhoons were in the north side of the Taiwan Strait. Accompanying with them, strong wind in the sea area north of the Taiwan Strait (remote wind) caused higher storm surge elevation in the north of the strait than that in the south (e.g., Figure 18c during Khanun), which produced a remarkable along-strait water level gradient. Thus, the remote wind effect was important in the southward transport events due to Khanun and Nabi. By contrast with the above two events, the event 4 due to Typhoon Damrey was induced by local wind stress term and the along-strait water level gradient has no contribution (Figure 17). Damrey was in the south side of the Taiwan Strait and the wind in the sea area north of the strait was weak, which resulted in a low storm surge elevation in the north of the strait (Figure 18d) and then an insignificant along-strait water level gradient between the two sections. In other words, there was little remote wind effect on the southward transport event 4. The local wind in the Taiwan Strait was obviously intensified by Damrey (Figure 3) and then the strong local wind was mainly responsible for the strong southward transport event due to Damrey.

7. Conclusion

[34] Both model simulations and buoy observations demonstrated that all five typhoons caused a strong southward current and then southward transport event in the Taiwan Strait during the period of 27 August to 5 October 2005. Typhoon-generated local wind stress and/or along-strait water level gradient were the direct forcing factors in the southward transport events. Even though Typhoon Nabi was far away from the Taiwan Strait, a perceptible southward transport event was generated by the along-strait water level gradient, which was related to the remote wind effect of the typhoon. According to the numerical results, the Coriolis force made a negative contribution to the southward transport events and the contribution of the along-strait momentum gradient (related to the advective term) was negligible.

[35] Typhoon generated a strong southward transport which, as an event of several days, reduced or even reversed the instantaneous northward transport in the Taiwan Strait. It would be valuable to investigate the influence of southward transport events due to typhoons on the monthly or

seasonal transport through the Taiwan Strait during the typhoon prevailing seasons in any future work.

Appendix A

[36] In the Cartesian coordinates, let x coordinate be directed to the northeast along the midline of the Taiwan Strait (Figure 2a) and y coordinate to the northwest across the strait. The origin of the system of coordinates is located on the undisturbed sea surface. The along-strait depth-averaged momentum equation and continuity equation can be written as follows:

$$\frac{\partial U}{\partial t}+U\frac{\partial U}{\partial x}+V\frac{\partial U}{\partial y}-fV=-g\frac{\partial \zeta}{\partial x}+\frac{F}{\rho H}, \tag{A1}$$

$$\frac{\partial \zeta}{\partial t}+\frac{\partial HU}{\partial x}+\frac{\partial HV}{\partial y}=0, \tag{A2}$$

where F is the combination of external compelling forces (wind stress, air pressure gradient force and bottom stress); U and V are the components of depth-averaged current in x direction and y direction, respectively. Other notations are the same as those described previously.

[37] If we multiply equation (A1) by H and use the fact of $\frac{\partial h}{\partial t}=0$, we obtain

$$\frac{\partial HU}{\partial t}=U\frac{\partial \zeta}{\partial t}-HU\frac{\partial U}{\partial x}-HV\frac{\partial U}{\partial y}-gH\frac{\partial \zeta}{\partial x}+\frac{F}{\rho}+fHV. \tag{A3}$$

Substituting in the continuity equation (A2), the equation can be rewritten as

$$\frac{\partial HU}{\partial t}=-\frac{\partial HU^2}{\partial x}-\frac{\partial HUV}{\partial y}-C^2\frac{\partial \zeta}{\partial x}+\frac{F}{\rho}+fHV, C=\sqrt{gH}. \tag{A4}$$

According to the definition, the transport through a section across the strait can be described as

$$Q=\int_{-b/2}^{b/2}HUdy, \tag{A5}$$

where b denotes the width of the strait at the section. Integrating equation (A4) for y from the eastern bank to the western bank and substituting in equation (A5) result in the following transport equation for the entire strait:

$$\frac{\partial Q}{\partial t}=-\frac{\partial}{\partial x}\int_{-b/2}^{b/2}HU^2dy-\int_{-b/2}^{b/2}\frac{\partial HUV}{\partial y}dy-\int_{-b/2}^{b/2}\left(C^2\frac{\partial \zeta}{\partial x}\right)dy+\int_{-b/2}^{b/2}\frac{F}{\rho}dy+\int_{-b/2}^{b/2}fHVdy. \tag{A6}$$

[38] The second term on the right-hand side is equal to zero based on the boundary condition that no water is allowed to flow through the coastal boundaries, assuming that both banks of the strait are approximately in parallel with the x coordinate. So the transport equation can be written as

$$\frac{\partial Q}{\partial t}=-\frac{\partial}{\partial x}\int_{-b/2}^{b/2}HU^2dy-\int_{-b/2}^{b/2}\left(C^2\frac{\partial \zeta}{\partial x}\right)dy+\int_{-b/2}^{b/2}\frac{F}{\rho}dy+\int_{-b/2}^{b/2}fHVdy. \tag{A7}$$

[39] **Acknowledgments.** This work was jointly supported by China Postdoctoral Science Foundation (20070420745), the Science Foundation of Fujian Province (2009J01223), and a project of the National High-Tech Research and Development Program (2006AA09A302–6). The buoy data were taken from the FOFB. The blended wind data were obtained from the CERSAT at IFREMER, Plouzané, France (http://cersat.ifremer.fr/layout/set/print/data/). The surface air pressure and current data were from the Physical Sciences Division of the Earth System Research Laboratory (http://www.cdc.noaa.gov/data/gridded/) and the Climate Prediction Center of the National Weather Service (http://www.cpc.ncep.noaa.gov/products/GODAS/), United States. The QuikSCAT wind data was taken from the California Institute of Technology of the NASA Jet Propulsion Laboratory, United States, and processed by the Group of Remote Sensing and Numerical Modeling, Xiamen University, China. The authors are grateful to Quanan Zheng, Yan Li, and Fengyan Shi for their valuable suggestions and to John Hodgkiss for polishing the English. We also appreciate two anonymous reviewers' helpful suggestions for the improvement of this paper.

References

Allen, J. S., and P. K. Kundu (1978), On the momentum, vorticity and mass balance on the Oregon Shelf, *J. Phys. Oceanogr.*, *8*, 13–27, doi:10.1175/1520-0485(1978)008<0013:OTMVAM>2.0.CO;2.

Chai, F., H. Xue, and M. Shi (2001), The study of horizontal transport in the Taiwan Strait, *Oceanogr. China*, *13*, 168–177.

Chuang, W.-S. (1985), Dynamics of subtidal flow in the Taiwan Strait, *J. Oceanogr. Soc. Jpn.*, *41*, 65–72, doi:10.1007/BF02109175.

Chung, S.-W., S. Jan, and K.-K. Liu (2001), Nutrient fluxes through the Taiwan Strait in spring and summer 1999, *J. Oceanogr.*, *57*, 47–53, doi:10.1023/A:1011122703552.

Fang, G., B. Zhao, and Y. Zhu (1991), Water volume transport through the Taiwan Strait and the continental shelf of the East China Sea measured with current meters, *Oceanography of Asian Marginal Seas*, edited by K. Takano, pp. 345–358, Elsevier, Amsterdam.

Fang, G., Z. Wei, B.-H. Choi, K. Wang, Y. Fang, and W. Li (2003), Inter-basin freshwater, heat and salt transport through the boundaries of the East and South China Seas from a variable-grid global ocean circulation model, *Sci. China Ser. D*, *46*, 149–161.

Fang, Y., G. Fang, K. Wang, and Z. Wei (2001), Dynamics of the Kuroshio intrusion into the Southeast China adjacent waters—A numerical study, *J. Hydrodyn. Ser. B*, *3*, 28–33.

Holland, G. J. (1980), An analytic model of the wind and pressure profiles in hurricanes, *Mon. Weather Rev.*, *108*, 1212–1218, doi:10.1175/1520-0493(1980)108<1212:AAMOTW>2.0.CO;2.

Jan, S., and S.-Y. Chao (2003), Seasonal variation of volume transport in the major inflow region of the Taiwan Strait: The Penghu Channel, *Deep Sea Res. Part II*, *50*, 1117–1126, doi:10.1016/S0967-0645(03)00013-4.

Jan, S., J. Wang, C.-S. Chern, and S.-Y. Chao (2002), Seasonal variation of the circulation in the Taiwan Strait, *J. Mar. Syst.*, *35*, 249–268, doi:10.1016/S0924-7963(02)00130-6.

Jelesnianski, C. P. (1965), A numerical calculation of storm tides induced by a tropical storm impinging on a continental shelf, *Mon. Weather Rev.*, *93*, 343–358, doi:10.1175/1520-0493(1993)093<0343:ANCOS>2.3.CO;2.

Ko, D. S., R. H. Preller, G. A. Jacobs, T. Y. Tang, and S. F. Lin (2003), Transport reversals at Taiwan Strait during October and November 1999, *J. Geophys. Res.*, *108*(C11), 3370, doi:10.1029/2003JC001836.

Tang, T. Y., J. H. Tai, and Y. J. Yang (2000), The flow pattern north of Taiwan and the migration of the Kuroshio, *Cont. Shelf Res.*, *20*, 349–371, doi:10.1016/S0278-4343(99)00076-X.

Wang, Y. H., S. Jan, and D. P. Wang (2003), Transports and tidal current estimates in the Taiwan Strait from shipboard ADCP observations (1999–2001), *Estuarine Coastal Shelf Sci.*, *57*, 193–199, doi:10.1016/S0272-7714(02)00344-X.

Wu, C.-R., and Y.-C. Hsin (2005), Volume transport through the Taiwan Strait: A numerical study, *Terr. Atmos. Oceanic Sci.*, *16*, 377–391.

Wu, C.-R., S.-Y. Chao, and C. Hsu (2007), Transient, seasonal and interannual variability of the Taiwan Strait current, *J. Oceanogr.*, *63*, 821–833, doi:10.1007/s10872-007-0070-1.

Wyrtki, K. (1961), Physical oceanography of the southeast Asian waters, *Naga Rep. 2*, pp. 1–195, Scripps Inst. of Oceanogr., San Diego, Calif.

Zhang, W.-Z. (2006), The study of typhoon surge and its numerical prediction model in the Taiwan Strait, Ph.D. dissertation, 168 pp., Xiamen Univ., Xiamen, China.

Zhang, W.-Z., H.-S. Hong, S.-P. Shang, D.-W. Chen, and F. Chai (2007), A two-way nested coupled tide-surge model for the Taiwan Strait, *Cont. Shelf Res.*, *27*, 1548–1567, doi:10.1016/j.csr.2007.01.018.

Zilang, F., H. Jianyu, and Y. Guoming (1991), Seawater flux through Taiwan Strait, *Chin. J. Oceanol. Limnol.*, *9*(3), 232–239, doi:10.1007/BF02850748.

F. Chai, School of Marine Sciences, University of Maine at Orono, 5706 Aubert Hall, Orono, ME 04469-5706, USA. (fchai@maine.edu)

H.-S. Hong (corresponding author) and W.-Z. Zhang, State Key Laboratory of Marine Environmental Science, Xiamen University, 422 Siming Nanlu, Xiamen 361005, China. (hshong@xmu.edu.cn; zwenzhou@xmu.edu.cn)

S.-P. Shang, Key Laboratory of Underwater Acoustic Communication and Marine Information Technology of the Minister of Education, Xiamen University, 422 Siming Nanlu, Xiamen 361005, China. (spshang@xmu.edu.cn)

X.-H. Yan, Center for Remote Sensing, College of Earth, Ocean, and Environment, University of Delaware, 209 Robinson Hall, Newark, DE 19716, USA. (xiaohai@udel.edu)